Elucidating white-etching matter through high strain-rate tensile testing

W. Solano-Alvarez[a], J. Duff[b], M. C. Smith[b], H. K. D. H. Bhadeshia[a]

[a] *Department of Materials Science and Metallurgy, University of Cambridge, U.K.*

[b] *Dalton Nuclear Institute, University of Manchester, U.K.*

Abstract

A form of damage in bearing steels subjected to rolling contact fatigue is the formation of localised regions of hard material just below the contact surface. These 'white-etching regions' are strikingly visible signs of damage during metallographic examination. One mechanism proposed to explain their formation is adiabatic shear localisation. Experiments are reported here using high strain-rate ($250\,s^{-1}$) tensile testing to show that this is not the case.

Keywords: 52100 bearing steel, white-etching matter, high strain rate tensile testing, adiabatic shear localisation, rolling contact fatigue

1. Introduction

White-etching matter (WEM) consists of nanostructured ferrite that forms in steels subjected to rolling contact fatigue [1–6]. It can have different morphologies, which can be harder or softer than the matrix depending on their carbon concentration. Harder types include surface layers, spheres, white-etching cracks, or 'butterfly' wings, while softer ones are low and high angle bands [7–10]. In the case of large bearings used in wind turbine gearboxes, white-etching cracks and wings can lead to their premature failure through a mechanism called white structure flaking; the subject has been reviewed extensively [5, 10–12].

One mechanism that has been suggested for the formation of the white

bands is adiabatic shear [13], which occurs when strain rates associated with localised plasticity in steels exceed about $10^2\,s^{-1}$ [14]. The mechanism requires that deformation is first initiated locally (for example at inclusions), but the high strain rate leads to the generation of heat that cannot be dissipated fast enough by diffusion into the surroundings. As a result the local region heats up and softens at a rate that is greater than any work hardening effect, thus exacerbating the strain localisation [15, 16]. This idea has been applied to a common bearing steel where white bands were observed in the microstructure following high strain-rate compression tests, leading to the conclusion that the normal white-etching bands, and possibly white-etching wings, that are observed in bearings are the result of adiabatic shear localisation [13].

However, an alternative interpretation is that the uniaxial compression causes the formation of cracks, and the crack faces then rub together under the influence of the compressive stress to form the white bands. In this interpretation, the damage by cracking must occur first, as has been demonstrated in rolling-contact experiments on bearing steels [12, 17–19]. In other words, the adiabatic bands per se are not the cause but the symptom of the damage mechanism.

To prove this, we report experiments where high strain-rate *tensile tests* are conducted to eliminate the possibility of crack faces rubbing against each other following the initial fracture event. Both uniaxial compression and uniaxial tension lead to the same shear stresses so the formation of the adiabatic shear bands should be insensitive to the type of applied stress.

2. Experimental Methods

2.1. Material

The material used is an Ovako hot-rolled and spheroidised 52100 steel rod with the following composition in weight percent:

0.98C-1.38Cr-0.28Mn-0.06Mo-0.28Si-0.18Ni

0.04Al-0.010P-0.017S-0.21Cu-0.015Co-0.001Ca-0.001Ti.

Flat tensile samples 2.5 mm thick, 160 mm long, and 20 mm wide were cut using an electric discharge machine along the rolling direction of the rod. The gauge section was 2.5 mm thick, 40 mm long, and 10 mm wide.

2.2. Heat treatments

Samples were individually wrapped in three layers of stainless steel foil, welded to a thermocouple to monitor the temperature, and heat treated in a standard Carbolite RWF1200 box furnace. All four samples were austenitised at 840 °C for 20 min and quenched in *GP460* oil at room temperature. Only half of the samples were then tempered, without the foil, at 160 °C for 2 h, which corresponds to the standard heat treatment for 52100 steel. Electron microscopy and vickers hardness measurements were performed to ensure the heat treatments created the desired microstructures and mechanical properties.

2.3. Tensile testing

Before testing, the samples were instrumented with 5 mm long ultrahigh-elongation Cu-Ni alloy foil strain gauges/sensors that have a resistance of 120.2±0.2 Ω and a gauge factor of 2.03±1.0% at 24 °C. The strain sensors were fixed to the centre of the gauge section of the sample with a cyanoacrylate base cement after slightly grinding the surface with a 320 SiC sandpaper. The wires of the strain sensor were soldered to a small terminal, glued outside the gauge section, and to the two 0.5 mm in diameter tinned copper conductors of a sensor cable that connected the strain sensor to the amplifier. The strain sensor, its wires and the terminal were then covered in a two component epoxy adhesive to prevent a short circuit or detachment during testing.

The instrumented samples were then placed between the clamps of a *Zwick/Roell Amsler HTM 5020* tensile testing machine operating at a test speed of $10\,\mathrm{m\,s^{-1}}$ and a measurement time of 32 ms. A speed of $20\,\mathrm{m\,s^{-1}}$ could not be used because the samples slipped off the clamps and due of their high hardness, damaged the knurling pattern of the grips.

2.4. Characterisation

After testing, samples were cut up and the fracture surfaces studied using an *Olympus* stereographic microscope and a *JEOL JSM 5500LV* scanning electron microscope (SEM) equipped with an *Oxford Instruments* EDS detector. The surface of the samples along the length and thickness of the gauge section in proximity to the fractured edge were then metallographically prepared and observed using using a *Zeiss* optical microscope (OM) and the SEM. These samples were ground and polished several times to observe the microstructure of the bulk at different depths with respect to the surface. Some micrographs were stitched together to provide a high-quality macroscopic perspective.

3. Results and Discussion

The average Vickers hardness values and standard errors based on twenty indentations close to the fractured edges are: 751±6 HV30 for sample 1-Q*, 799±2 HV30 for sample 2-Q, 778±2 HV30 for sample 3-Q, and 700±4 HV30 for sample 4-QT. Since each sample was heat treated individually, the differences in hardness are attributed to how tightly the foil was wrapped around each sample, which affects the heat conduction when inside the furnace and during the quench.

The speed of the cross head created a strain rate of $250\,\mathrm{s}^{-1}$ at the gauge section that initiated fracture most likely at surface imperfections or surface inclusions and propagated in a direction normal to the applied stress, as shown in fig. 1. Despite the lack of tempering of samples 1-Q and 3-Q, the fracture topography indicates ductile cleavage. At high magnifications, a characteristic mottled pattern and many examples of intergranular fracture can be seen (fig. 2a). In sample 3-Q, one of the corners showed a collection of bright spots under the OM, which were suspected to be cross sections of adiabatic shear bands. Further analysis using the SEM showed a more brittle fracture surface at these spots compared to the matrix, as seen in fig. 2b. Nevertheless, EDS measurements confirmed these regions to be

*Q stands for quenched and QT for quenched and tempered

enriched in sulphur (2.91±.18 wt%) and manganese (2.76±0.19 wt%) in addition to chromium (1.65±0.27 wt%) and iron (92.67±0.36 wt%), suggesting the spots are simply a family of manganese sulphide inclusions, broken down during rolling. Their presence was confirmed by the thickness profile shown in fig. 2d.

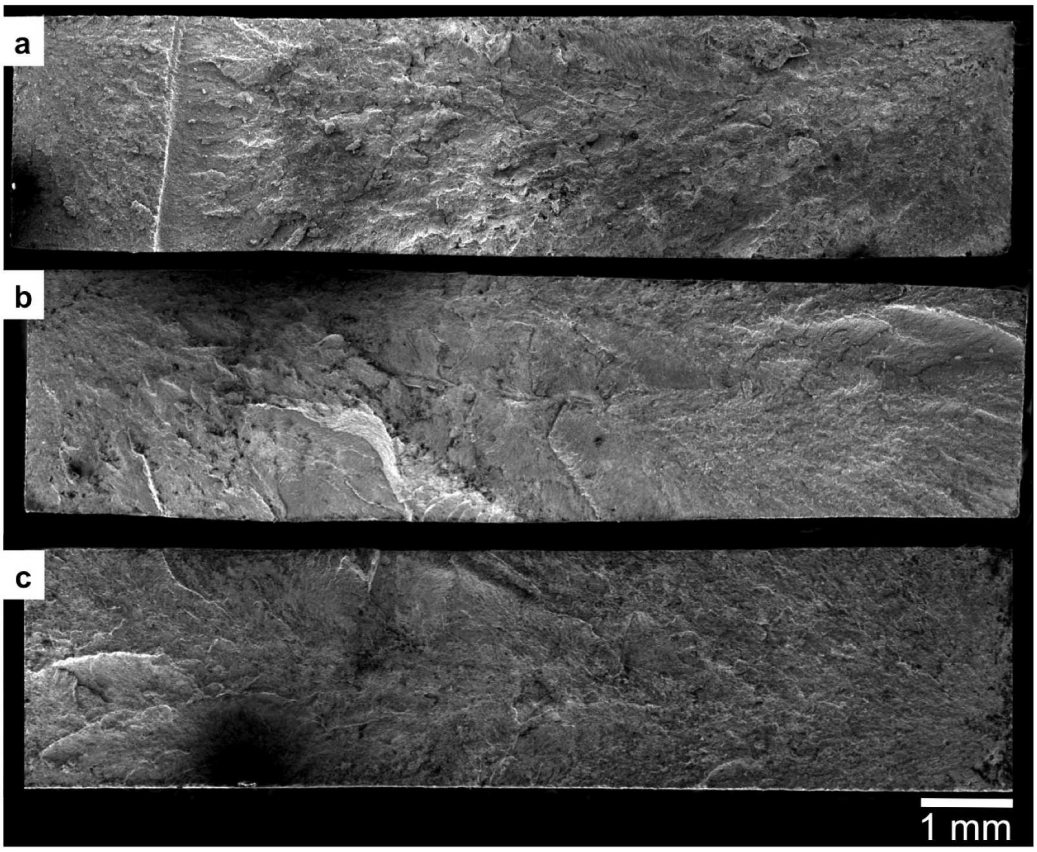

Figure 1: Stitched SEM micrographs of the fracture surfaces of samples: a) 1-Q, b) 3-Q, and c) 4-QT.

The microstructure of the lateral (along the length) and thickness profiles are presented in fig. 3. The uneven surfaces of the profiles confirm ductile cleavage in all samples, irrespective of heat treatment. The microstructure reveals a strong presence of segregation bands, more evident under the optical microscope, but no sign of adiabatic shear bands or white-etching bands, even at high magnifications, different depths with respect to the surface, and

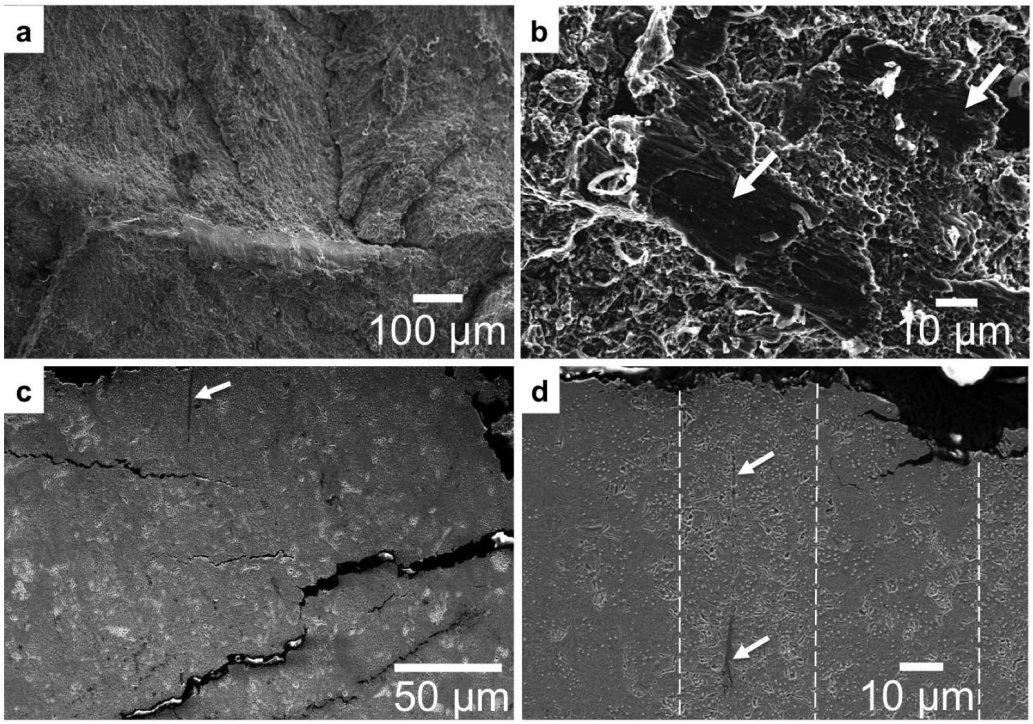

Figure 2: Higher magnification SEM micrographs of: a) fracture surface of 3-Q, b) two of the bright spots found in 3-Q indicated by white arrows, c) surface along length of sample 1-Q in proximity to the fractured edge showing cracks at 45 ° to the fracture surface, which is the angle of maximum shear stress and a MnS inclusion pointed by an arrow, d) thickness profile of 3-Q showing that MnS inclusions, pointed by arrows, and granular carbides are more common inside the segregation bands outlined by the dashed lines.

etched or unetched conditions (fig. 2c and 2d). It would be expected to find adiabatic shear bands following the lines of maximum shear stress or slip planes [15], such as the cracks shown in fig. 2c, but such was not the case. The lack of ASB seems to be caused by the tensile stress applied and the ductile cleavage failure mode, which does not allow for cracks in the bulk of the sample to form and then rub their surfaces against each other under the generated shear stresses, as it happens under compression. This fact suggests that adiabatic shear localisation cannot describe the appearance of white-etching cracks or white-etching wings. Instead, the more appropriate mechanism seems to be the frictional contact of broken surfaces within the bulk that reduce the local compliance and causes intense localised deformation [19, 20].

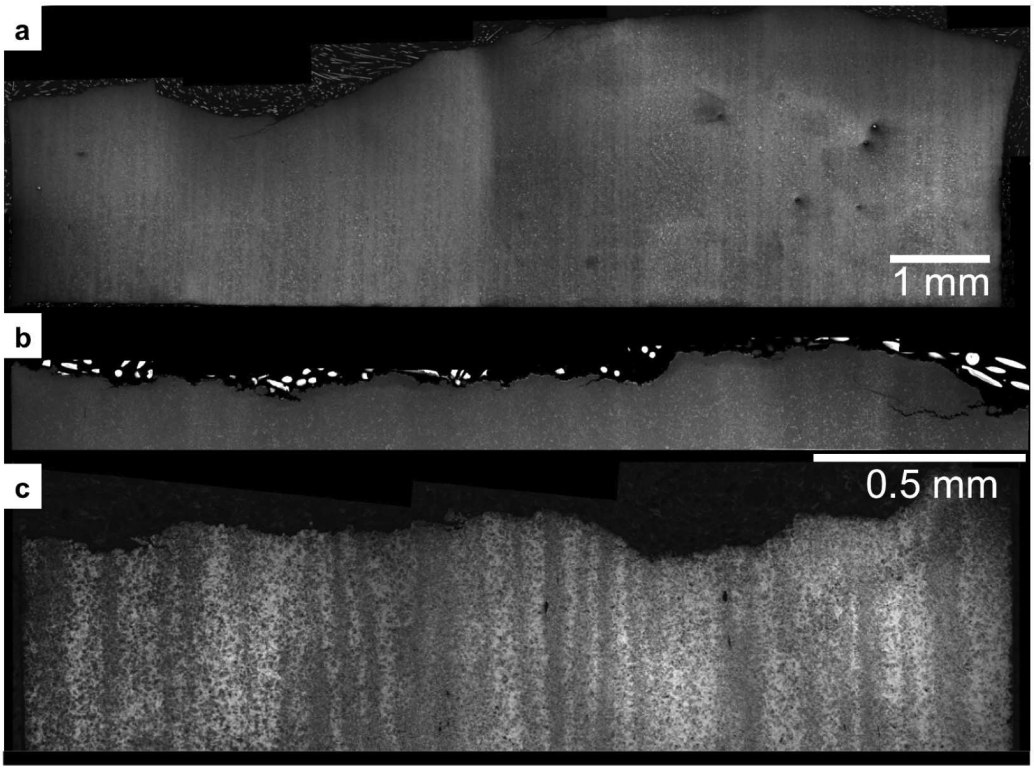

Figure 3: Stitched micrographs showing: a) surface along length of 1-Q (SEM), b) surface along thickness of 3-Q (SEM), and c) same sample as as b) after further grinding (OM). b) and c) share the same magnification.

4. Conclusions

High strain rate tensile testing of quenched, and quenched and tempered bearing steel revealed no signs of adiabatic shear banding, like those reported for compressive stress. This fact serves as evidence to question the adiabatic shear localisation theory for the formation of white-etching matter in bearing steels subjected to rolling contact fatigue. Instead, the more likely mechanism responsible for the formation of hard types of white-etching matter such as white-etching cracks and white-etching butterfly wings seems to be the beating/rubbing of crack faces under the resulting shear stresses of either compressive loading or rolling contact fatigue that lead to a reduction of local compliance and increased localised deformation. This proposed mechanism instead, does explain why white-etching matter can be seen in high strain rate compressive tests where cracks can be rubbed against each other, but not in equivalent tensile tests.

The corollary of this work is that adiabatic shear bands and white-etching matter form by distinct mechanisms, at different scales, and under significantly different strain and strain rates.

5. Acknowledgements

Funding by CONACyT, the Cambridge Overseas Trust, and the Roberto Rocca Education Programme is highly appreciated and acknowledged. We are grateful to A. W. Rayment of the Mechanical Testing Laboratory for his help with sample instrumentation.

6. References

References

1. R. Tricot, J. Monnot, and M. Lluansi: 'How microstructural alterations affect fatigue properties of 52100 steel', *Metals Engineering Quarterly*, 1972, **12**, 39–47.

2. A. Grabulov, U. Ziese, and H. W. Zandbergen: 'TEM/SEM investigation of microstructural changes within the white etching area under rolling contact fatigue and 3-D crack reconstruction by focused ion beam', *Scripta Materialia*, 2007, **57**, 635–638.

3. K. Hiraoka: 'White-type microstrutural change in rolling contact fatigue from the veiwpoint of severe plastic deformation', *Tetsu-to-Hagane*, 2008, **94**, 636–643.

4. A. Grabulov, R. Petrov, and H. W. Zandbergen: 'EBSD investigation of the crack initiation and TEM/FIB analyses of the microstructural changes around the cracks formed under rolling contact fatigue', *International Journal of Fatigue*, 2010, **32**, 576–583.

5. M.-H. Evans: 'White structure flaking in wind turbine gearbox bearings: effects of 'butterflies' and white etching cracks', *Materials Science and Technology*, 2012, **28**, 3–22.

6. J. H. Kang, B. Hosseinkhani, and P. Rivera: 'Rolling contact fatigue, bearing steels, multiscale modelling, kinetics, microstructure control, fatigue', *Materials Science and Technology*, 2012, **28**, 44–49.

7. J. M. Beswick: 'Measurement of carbon levels in structurally transformed SAE 52100 ball bearing steel by microprobe analysis', *Practical Metallography*, 1975, **12**, 200–206.

8. R. Österlund, M. Aucouturier, and O. Vingsbo: 'High resolution autoradiography determination of carbon diffusion during rolling contact fatigue in ball bearings', *Scandinavian Journal of Metallurgy*, 1981, **10**, 67–72.

9. N. Mitamura, H. Hidaka, and S. Takaki: 'Microstructural development in bearing steel during rolling contact fatigue', *Materials Science Forum*, 2007, **539-543**, 4255–4260.

10. H. K. D. H. Bhadeshia: 'Steels for bearings', *Progress in Materials Science*, 2012, **57**, 268–435.

11. R. Errichello, R. Budny, and R. Eckert: 'Investigations of bearing failures associated with white etching areas (WEAs) in wind turbine gearboxes', *Tribology Transactions*, 2013, **56**, 1069–1076.

12. H. K. D. H. Bhadeshia, and W. Solano-Alvarez: 'Critical assessment 13: Elimination of white etching matter in bearing steels', *Machining Science and Technology*, 2015, **31**, 1011–1105.

13. H. Schlicht: 'About adiabatic shear bands and the generation of "high-angle white bands" in roller bearings', *Materialwissenschaft und Werkstofftechnik*, 2008, **39**, 217–226.

14. K. Ryttberg, M. K. Wedel, V. Recina, P. Dahlman, and L. Nyborg: 'The effect of cold ring rolling on the evolution of microstructure and texture in 100Cr6 steel', *Materials Science & Engineering A*, 2010, **527**, 2431–2436.

15. Y. Bai, and B. Dodd: Adiabatic Shear Localization: Occurrence, Theories and Applications: Oxford, U. K.: Pergamon Press, 1992.

16. S. M. Walley: 'Shear localisation: a historical overview', *Metallurgical & Materials Transactions A*, 2007, **38A**, 2629–2654.

17. K. Hiraoka, M. Nagao, and T. Isomoto: 'Study of flaking process in bearings by white etching area generation', *Journal of ASTM International*, 2007, **3**, 234–240.

18. W. Solano-Alvarez, and H. K. D. H. Bhadeshia: 'White-etching matter in bearing steel. Part 1: Controlled-cracking of bearing steel', *Metallurgical & Materials Transactions A*, 2014, **45**, 4907–4915.

19. W. Solano-Alvarez, and H. K. D. H. Bhadeshia: 'White-etching matter in bearing steel: Part II: distinguishing cause and effect in bearing steel failure', *Metallurgical & Materials Transactions A*, 2014, **45**, 4916–4931.

20. P. M. Anderson, N. A. Fleck, and K. L. Johnson: 'Localization of plastic deformation in shear due to microcracks', *Journal of the Mechanics and Physics of Solids*, 1990, **38**, 681–699.